

1 **Projected Changes in Hot, Dry and Compound Hot-Dry Extremes over Global Land**
2 **Regions**
3

4 Paolo De Luca¹ and Markus G. Donat^{1,2}

5 ¹Barcelona Supercomputing Center (BSC), Barcelona, Spain

6 ²Institució Catalana de Recerca i Estudis Avançats (ICREA), Barcelona, Spain

7
8 Corresponding author: Paolo De Luca (paolo.deluca@bsc.es)
9

10 **Key Points:**

- 11 • Hot extremes are projected to increase in frequency and intensity over almost all land
12 areas by the end of the 21st century.
- 13 • Drought changes depend on measure but increase robustly over central and northern
14 South America, the Mediterranean and southern Africa.
- 15 • Compound hot and dry extremes are sensitive to the drought measure but projected to
16 increase in most regions globally.

17 **Abstract**

18 The impacts of hot, dry and compound hot-dry extremes are significant for societies, economies
19 and ecosystems worldwide. Such events therefore need to be assessed in the light of
20 anthropogenic climate change so that suitable adaptation measures can be implemented by
21 governments and stakeholders. Here we show a comprehensive analysis of hot, dry and
22 compound hot-dry extremes over global land regions using 25 CMIP6 models and four future
23 emissions scenarios from 1950 to 2100. Hot, dry and compound hot-dry extremes are projected
24 to increase over large parts of the globe by the end of the 21st century. Hot and compound hot-
25 dry extremes show the most widespread increases and dry extreme changes are sensitive to the
26 index used. Many regional changes depend on the strength of greenhouse-gas forcing, which
27 highlights the potential to limit the changes with strong mitigation efforts.

28

29 **Plain Language Summary**

30 Heatwaves, drought and their joint occurrences can negatively impact populations, economies
31 and natural systems worldwide. It is therefore of paramount importance that governments and
32 stakeholders assess the risk from such events and adapt accordingly. In this study we use 25
33 climate models and four emission scenarios from 1950 to 2100 to assess how hot, dry and
34 compound hot-dry extremes are expected to change in the future when compared to current
35 climate conditions. We find that such extremes are projected to increase by the end of the 21st
36 century over large parts of global land areas under the highest-emission, no-policy, climate
37 change scenario. Hot and compound hot-dry extremes show the most widespread increases,
38 whereas dry extreme changes are sensitive and more regionally-limited depending on the method
39 by which they are computed. Most of the regional changes in hot, dry and compound hot-dry
40 extremes can be reduced with strong climate change mitigation efforts to limit future green-
41 house gas emissions.

42

43

44 **1 Introduction**

45 Socio-economic and environmental impacts of hot, dry and compound hot-dry meteorological
46 extremes can pose a significant distress to natural and socio-economic systems worldwide
47 (Barriopedro et al., 2011; Zscheischler et al., 2018; Zscheischler & Fischer, 2020). It is therefore
48 of paramount importance to provide information on how these meteorological hazards may
49 change in the future under anthropogenic climate change.

50

51 Hot and dry extremes can occur concurrently (or within a time-frame of a few weeks) at a
52 location (Bevacqua et al., 2022; Hao et al., 2018; Manning et al., 2019; Mukherjee et al., 2022,
53 2023; Zscheischler et al., 2018, 2020) and at present, there are no metrics for computing
54 compound hot-dry extremes which gathered the same importance as for example the Climpact
55 indices for univariate extremes (<https://climpact-sci.org/>). This is because research on compound
56 extremes is a relatively new field of investigation and also because compound events can be
57 quantified in many different ways, for example occurring simultaneously or subsequently, at the
58 same location or at different locations (e.g. De Luca, Messori, Pons, et al., 2020; De Luca,
59 Messori, Wilby, et al., 2020), so that the analysis remains complex, hindering a broader
60 consensus about which aspect of compound extremes matters most for a certain application.
61 However, some studies developed pragmatic indices and metrics for hot-dry extremes. Examples
62 are X. Wu et al. (2019) who developed a dry-hot magnitude index, Zhang et al. (2022) who

63 assessed compound agricultural droughts and hot events, Bevacqua et al. (2022) who defined
64 compound hot-dry events based on temperature and precipitation mean values within the warm
65 season and Ganguli (2023) who explored compound warm-dry events in India by developing an
66 index based on (warm) temperature, (lack of) precipitation and (low) wind-speed.
67

68 There is now a general consensus about a global increase in hot extremes under anthropogenic
69 climate change (e.g. Christidis et al., 2015; Fischer & Schär, 2010; Perkins-Kirkpatrick & Lewis,
70 2020), with such trend mainly attributed to thermodynamic changes, or to an increase in global
71 mean temperature (Rastogi et al., 2020; Vogel, Zscheischler, et al., 2020) and local land-
72 atmosphere feedbacks (Donat et al., 2017; Seneviratne et al., 2006), with also changes in the
73 atmospheric circulation playing a role for example in Eurasia and North America (Horton et al.,
74 2015; Rousi et al., 2022; Schielicke & Pfahl, 2022; Suarez-Gutierrez et al., 2020). Future
75 projected changes in drought are sensitive to the index used (Cook et al., 2018; Dai, 2011, 2013).
76 This is because drought can be computed from precipitation alone (McKee et al., 1993) and also
77 from the combination of precipitation and potential evapotranspiration (PET) (Palmer, 1965;
78 Vicente-Serrano et al., 2010), with the latter case taking into account the effect of increasing
79 temperatures. Future changes in drought based on precipitation deficit point toward an increase
80 in dryness over northern South America, the Mediterranean, southern Africa and South Australia
81 (Ukkola et al., 2020). On the other hand, projections of drought computed from precipitation and
82 PET show increased dryness over the same regions as Ukkola et al. (2020) and also in Central
83 and central-north America, most of the African continent, central Europe, the Middle East,
84 southeast Asia and Australia (Dai, 2011, 2013). Lastly, changes in drought can be also sensitive
85 to the equation used to approximate PET, as shown in Begueria et al. (2014). Other factors
86 playing a role in shaping drought events in the short-term over some of these regions are sea-
87 surface temperatures anomalies, weakened summer Asian monsoons and likely changes in
88 atmospheric circulation patterns (Dai, 2011, 2013; Schubert et al., 2016; Teuling et al., 2013;
89 Trenberth et al., 2014). Lastly, and reflecting the changes in hot and dry extremes, also
90 compound hot-dry extremes are set to increase under anthropogenic climate change (Bevacqua et
91 al., 2022; Ridder et al., 2022; Vogel, Hauser, et al., 2020) and they appear to be modulated by
92 mean precipitation trends (Bevacqua et al., 2022). Most of these studies consider hot, dry and
93 hot-dry compound extremes separately, hindering a robust understanding of how these types of
94 extremes relate to each other. Moreover, they do not use different metrics for the computation of
95 dry extremes, also on several accumulation periods, such as indices that consider precipitation
96 and precipitation along with evaporative water demand, that can in turn affect dry and compound
97 hot-dry extreme changes.
98

99 Here we build on these works and provide a comprehensive analysis of projected changes in hot,
100 dry and compound hot-dry extremes over global land regions. We use a multi-model ensemble
101 (MME) of 25 Coupled Model Intercomparison Project Phase 6 (CMIP6) models (Eyring et al.,
102 2016), four emission scenarios, and a suite of different univariate and compound extreme
103 indices. Such indices consider different aspects of drought, such as precipitation and evaporative
104 water demand over multiple accumulation periods, also in compound extremes, which in
105 combination allows us to discuss how the changes in compound extremes relate to their
106 univariate hot and dry contributions.
107

108 **2 Data and Methods**

109 **2.1 Data**

110 We use CMIP6 data (Eyring et al., 2016), namely historical and future Scenario Model
111 Intercomparison Project (ScenarioMIP) (O'Neill et al., 2016) simulations. From the
112 ScenarioMIP we use four Shared Socioeconomic Pathways (SSPs): SSP1-2.6, SSP2-4.5, SSP3-
113 7.0 and SSP5-8.5. From these simulations we extract daily maximum near-surface temperature
114 (t_{max} , K), daily minimum near-surface temperature (t_{min} , K) and daily precipitation (pr ,
115 $kg \cdot m^{-2} \cdot s^{-1}$), respectively for the periods 1950-2014 and 2015-2100, for a MME of 25 models
116 (Table S1). From each model we only considered the first ensemble member available (in most
117 cases $r1i1p1f1$) so that models' structural uncertainty is taken into account (Deser, 2020).

118

119 **2.2 Climpact indices**

120 We compute a selection of extreme indices to quantify global hot and dry extremes from 1950 to
121 2100, using 1981-2010 as a baseline period for the calculation of percentile thresholds. The
122 indices are computed starting in 1949 to avoid obtaining incomplete index calculations in 1950
123 for indices that accumulate across calendar years, namely the Standardized Precipitation Index
124 (SPI, McKee et al., 1993) and Standardized Precipitation Evapotranspiration Index (SPEI,
125 Vicente-Serrano et al., 2010). For hot extremes we calculate the percentage of days when daily
126 maximum temperature exceeds the 90th percentile ($tx90p$) and the annual maximum of daily
127 maximum temperatures (txx) (Zhang et al., 2011). We also calculate three indices measuring
128 heatwave characteristics, where heatwaves are considered as periods of at least 3 consecutive
129 days when daily maximum temperatures exceed the 90th percentile (Perkins & Alexander,
130 2013). The heatwave amplitude (hwa_{tx90}) represents the annual peak daily value ($^{\circ}C$) in the
131 hottest heatwave, the heatwave duration (hwd_{tx90}) refers to the length (days) of the longest
132 heatwave within a year and heatwave frequency (hwf_{tx90}) measures the number of days within
133 a year that contribute to heatwaves (<https://climpact-sci.org/>).

134

135 To quantify the occurrence of dry extremes we use the SPI and SPEI with 3-, 6- and 12-month
136 accumulation periods. The SPI provides information about meteorological drought in terms of
137 lack of precipitation, whereas the SPEI in terms of lack of water availability by considering also
138 the atmospheric water demand. SPI and SPEI include the entire precipitation, or precipitation
139 minus PET, distributions, and do not directly indicate drought occurrences. A caveat is that PET
140 may overestimate drought in very dry regions, where actual evapotranspiration may be lower
141 than PET due to lack of water. We define drought when these monthly index values are ≤ -1 ,
142 which represents moderate drought conditions. We use -1 as threshold to ensure a sufficient
143 number of monthly values within the SPI and SPEI drought datasets, but lower values could be
144 used as criterion for more severe drought. As a baseline for the estimation of the distribution
145 parameters we use the entire investigation period (151 years, 1950-2100) (Vicente-Serrano et al.,
146 2020), to avoid potential biases outside relatively short reference periods as reported for example
147 by Sippel et al. (2015). To allow comparison across SSPs, we use the SPI and SPEI distribution
148 parameters derived for the Historical and one SSP scenario (i.e. SSP1-2.6) to compute SPI and
149 SPEI in the other scenarios. We use SSP1-2.6 because this is the scenario with smallest forcing
150 changes. For the SPEI we compute PET following Hargreaves (1994), which is based on
151 maximum and minimum temperatures (K), and latitude to estimate extraterrestrial radiation.
152 SPEI results can be sensitive to how PET is calculated (e.g. Beguería et al., 2014). Therefore, we
153 assess the sensitivity of SPEI to different PET approximations, i.e. following Thornthwaite
154 (1948), and the more complex Penman method (Allen et al., 1994). We perform this comparison
155 for two CMIP6 models, under SSP5-8.5 and SSP2-4.5, for $spei3$, $spei6$ and $spei12$. We find that
156 annual global mean time-series are in agreement between the Hargreaves and Penman methods,

157 but using the Thornthwaite method results in much stronger drying (Figures S1-S2). Similarly,
 158 for the drought occurrence measured as *spei3_dry*, *spei6_dry* and *spei12_dry* there is good
 159 agreement between calculations using the Hargreaves and Penman methods, but a stronger and
 160 more wide-spread increase in drought occurrence is found with the Thornthwaite method
 161 (Figures S3-S6). For the analysis of the full MME we therefore calculate PET using the
 162 Hargreaves method which gives relatively similar results to the more complex Penman
 163 approximation but requires less data. We use the index names *spiN_dry* and *speiN_dry* to refer to
 164 the count of dry months, where *N* stands for the accumulation period of the index (i.e. 3, 6 and
 165 12 months).

166 **2.3 Compound extremes**

167 We also compute indices that measure the occurrence of (same-day) compound hot-dry
 168 extremes. We define this index as *cex_d*, which stands for “compound extreme days”. Here we
 169 use tasmax extremes exceeding the 90th percentile (similar to *tx90p*, as indicator for hot
 170 extremes), SPI and SPEI (3, 6 and 12-month) monthly values ≤ -1 (as indicator for dry
 171 extremes). The tasmax percentiles are computed from SSP1-2.6 during the entire 1950-2100
 172 period, to make it consistent with the SPI and SPEI baselines, and serve as threshold for extreme
 173 temperatures in all SSP scenarios. In order to homogenize the temporal frequencies of the
 174 datasets, the SPI and SPEI original monthly time-series are converted into daily time-series by
 175 setting each daily value to the SPI and SPEI monthly value in which the day occurs.
 176

177
 178 The *cex_d* index assesses the occurrence of same-day compound hot-dry extremes and is
 179 computed as follows: i) identify daily hot extremes (tasmax >90th percentile) and daily dry
 180 extremes (SPI and SPEI ≤ -1); ii) count the number of days with compound (same-day) hot-dry
 181 extremes or when the hot days coincide with the occurrence of dry days. We name compound
 182 extremes calculated with SPI ≤ -1 as *cex_d (spiN)* and compound extremes computed with SPEI
 183 ≤ -1 as *cex_d (speiN)*, where *N* stands for the number of accumulated months (i.e. 3, 6 or 12).
 184

185 **2.4 Statistical analysis**

186 We calculate all the indices on the native CMIP6 model grids and then re-grid them to a common
 187 latitude-longitude grid of $2^\circ \times 2^\circ$ so that MME medians and percentiles can be computed across
 188 all models. We then remove the ocean grid-points with a land-sea mask in order to retain only
 189 land values and exclude Antarctica. Then, for each index we compute the MME median along
 190 with the MME interquartile range (25th and 75th percentiles), the latter used as a measure of inter-
 191 model uncertainty.
 192

193 To discuss the projected changes in extremes, we present annual global average time-series
 194 (weighted by gridpoint area) and maps of end-of-century changes relative to recent climate
 195 conditions. In the former we assess the MME medians using the modified Mann-Kendall test that
 196 takes into account autocorrelation (Hamed & Ramachandra Rao, 1998) and also compute the
 197 Sen’s slopes of the time-series (Sen, 1968). From the modified Mann-Kendall test we extract the
 198 p-values of the MME median trends. We calculate the maps of changes by taking the difference
 199 of MME medians (computed from single-model 20-year averages) between two periods, namely
 200 the four future SSPs during 2081-2100 and the historical simulations during 1981-2000. We
 201 assess the statistical significance of the resulting end-of-century changes, for each grid-point,
 202 with a two-tailed Wilcoxon rank-sum test (Mann & Whitney, 1947) that assesses if the median
 203 values are significantly different and does not assume data normally distributed. Then, we further

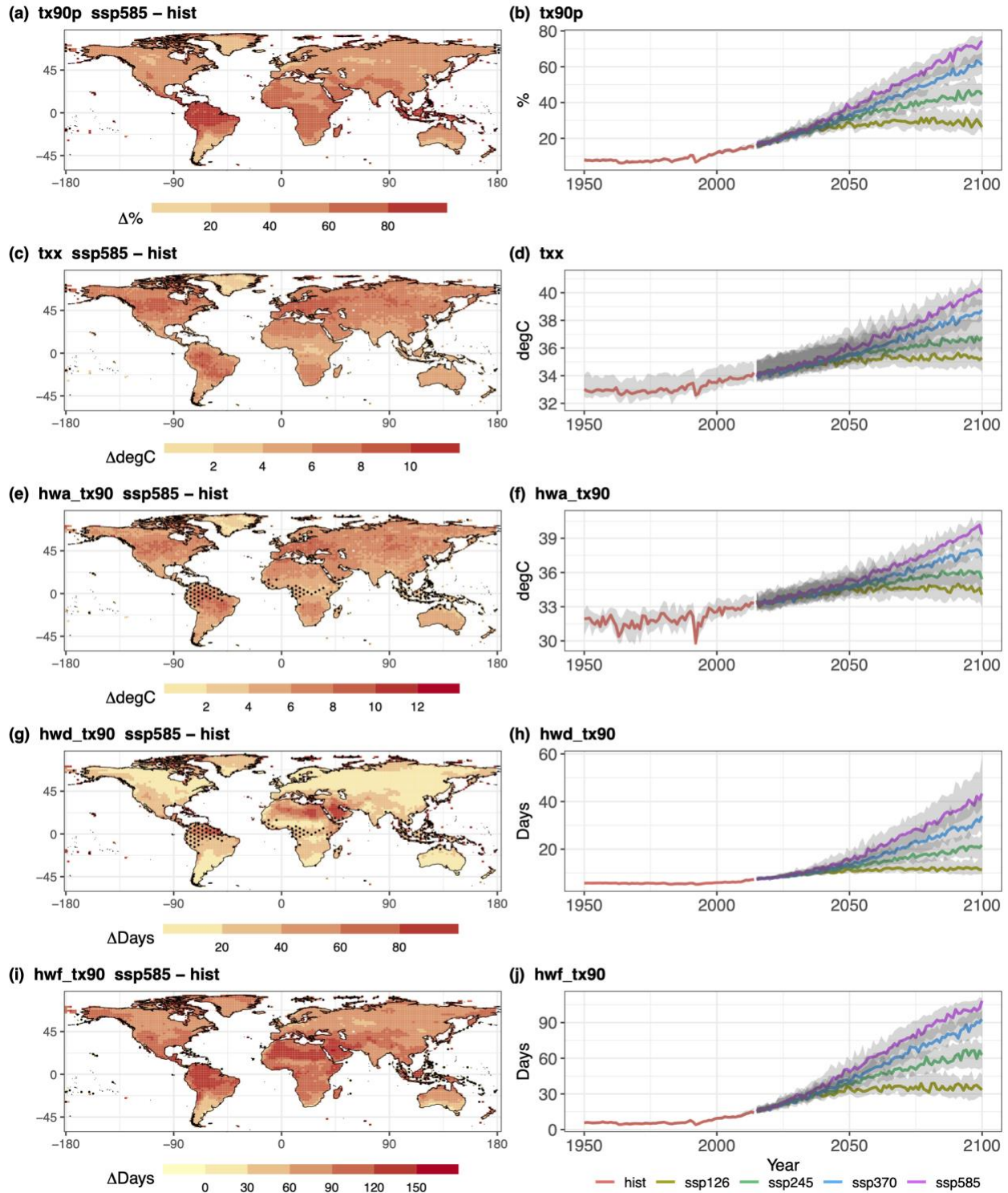
204 correct the p-values obtained with a Bonferroni correction (Bonferroni, 1936; Sedgwick, 2014)
205 that takes into account Type I errors (or false positives) in relation to multiple testing.
206

207 As a further assessment to indicate the robustness of the simulated changes across models, we
208 also apply a sign-test, which tests for each gridpoint if at least 80% (n=20) of models have a
209 difference value of the same sign (positive or negative).
210

211 **3 Simulated changes in extremes**

212 **3.1 Hot extremes**

213 The difference maps for SSP5-8.5 show widespread significant ($p < 0.05$) increases in the
214 different hot extremes indices, consistent with a warming climate (Figure 1a,c,e,g,i). The *tx90p*
215 index shows pronounced increase in the frequency of hot extremes over northern South America,
216 western, central and eastern Africa, the Arabian peninsula, the Tibetan plateau and Indonesia
217 (Figure 1a), whereas *txx* shows largest increases in the intensity of hot extremes over central
218 South America, central north America and Europe (Figure 1c). The *hwa_tx90* shows global
219 relatively homogeneous patterns of increased heatwave amplitude, however with largest
220 increases over central north America, parts of Brazil and Europe (Figure 1e). The *hwd_tx90*
221 index points toward substantial increase in the duration of heatwaves over northern Africa and
222 the Arabian peninsula (Figure 1g), whereas the *hwf_tx90* index shows overall large increases in
223 heatwave frequency, especially over northern and central parts of South America, northern
224 Africa, the Arabian peninsula and Indonesia (Figure 1i). Similar spatial patterns of projected
225 changes by the end of the 21st century, although less pronounced in terms of statistical
226 significance and magnitude, are obtained for the other SSP scenarios (Figure S7-S11). The
227 smaller increases in the lower-forcing scenarios (i.e. SSP1-2.6, SSP2-4.5 and SSP3-7.0) point out
228 the benefits of implementing strong mitigation measures (O'Neill et al., 2016). Looking at the
229 global average time-series, the MME of historical climate simulations shows relatively slow
230 increase during the late 20th and early 21st centuries, as compared to the future high-forcing SSP
231 scenarios. The historical simulations also show substantial reductions for the duration of 1-2
232 years in particular in the global average intensity of heat extremes (e.g. *txx* and *hwa_tx90*) in
233 response to, for example, the Pinatubo volcanic eruption in 1991 (Figure 1b,d,f,j). In the future
234 projections, all indices point towards increases in hot extremes, with SSP5-8.5 being the scenario
235 with most pronounced increases, SSP1-2.6 being the one with more moderate changes, and
236 SSP2-4.5 with SSP3-7.0 lying between the two (Figure 1b,d,f,h,j, $p < 0.01$, Table S2) - indicating
237 proportionality between the magnitude of change and the strength of the forcing (Seneviratne et
238 al., 2016).
239



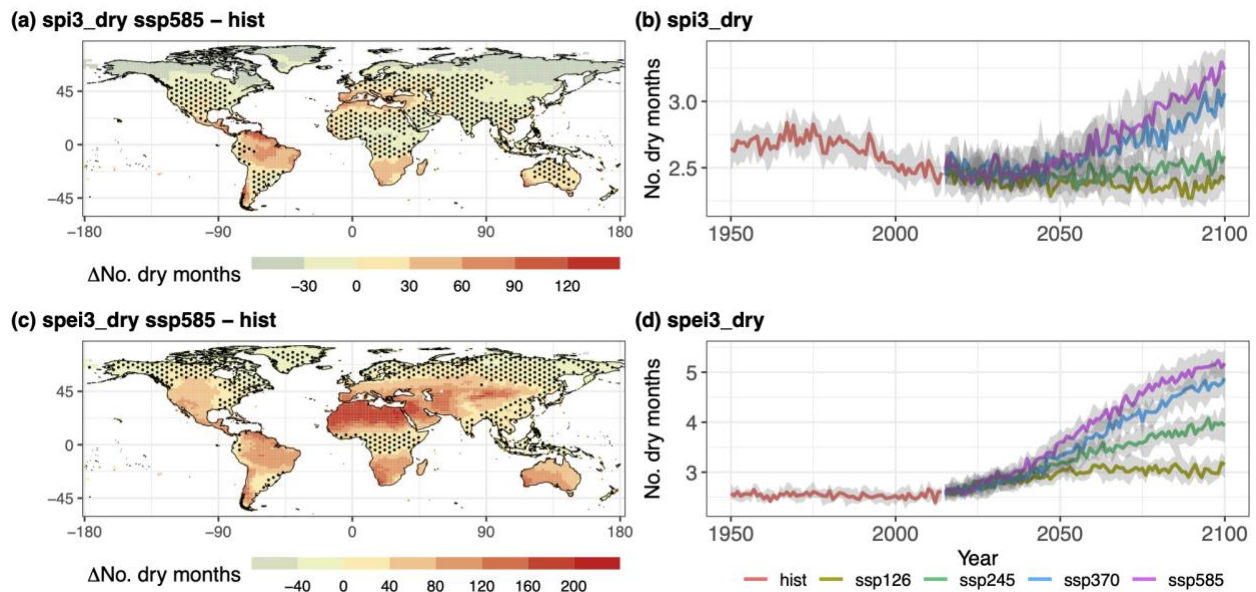
240
241
242
243
244
245
246

Figure 1. MME difference maps and global land average time-series of hot extremes. Maps show MME median changes between the SSP8-8.5 2081-2100 and historical 1981-2000 time slices, and time-series show MME medians (coloured lines) and interquartile ranges (grey shading) for the historical and SSP scenarios. (a)-(b) *tx90p*; (c)-(d) *txx*; (e)-(f) *hwa_tx90p*; (g)-(h) *hwd_tx90p*; and (i)-(j) *hwf_tx90p*. In (a,c,e,g,i) stippling indicates gridpoints where the difference is not statistically significant ($p \geq 0.05$) or that did not pass the sign-test ($\leq 80\%$).

247
 248
 249
 250
 251
 252
 253
 254
 255
 256
 257
 258
 259
 260
 261
 262
 263
 264
 265
 266
 267
 268
 269
 270
 271

3.2 Drought

Results for global dry extremes (Figure 2) differ depending on index, and therefore atmospheric variables taken into consideration, as also shown by Cook et al. (2018). The end-of-century changes for *spi3_dry* under SSP5-8.5 point toward both drying and wetting in different regions across the globe, reflecting e.g. annual mean precipitation changes reported by the IPCC AR6 (Masson-Delmotte et al., 2021; Figure SPM.5c). Hence, we find a significant ($p < 0.05$ and sign-test $> 80\%$) projected increase in drought occurrence (based on SPI) in central and South America, the Mediterranean basin, southern Africa and western Australia. Whereas drought occurrence is projected to decrease over China and in high northern latitudes (e.g. Alaska, Canada, Scandinavia and Russia; Figure 2a). Such heterogeneity in the difference maps is reflected in the global average time-series, which show a non-linear trend that cannot be assessed with a Slope value (Figure 2b). Specifically, the *spi3_dry* values of the historical period increase from 1950 to about the 1970s and then decrease until the end of the historical forcing runs in 2014. Following the historical period the global average *spi3_dry* values for SSP5-8.5 and SSP3-7.0 increase until the end of the 21st century, with the former showing the strongest upward trend, while the SSP2-4.5 and SSP1-2.6 global average time series remain relatively stationary (Figure 2b). However, although some global average time-series are showing little changes, the regional patterns of drying and wetting still remain in place (Figures S12-S13), but compensate each other in the global average. The results suggest that at stronger forcing levels (SSP5-8.5 and SSP3-7.0) the drought increases found in some tropical and subtropical regions overcompensate the drought decreases in the high northern latitudes.



272
 273 **Figure 2.** MME difference maps and global land average time-series of dry extremes. (a)-(b) Annual
 274 count of dry months computed with SPI 3-month index (*spi3_dry*); (c)-(d) annual count of dry months
 275 computed with SPEI 3-month index (*spei3_dry*). Time-periods, stippling and time-series colors are as in
 276 Figure 1.

277
 278

279 The picture is different when considering the count of dry months computed from SPEI and
280 therefore by taking into account PET along with precipitation (*spei3_dry*; Figure 2c,d). Here, the
281 end-of-century changes for SSP5-8.5 project a drying over much larger areas compared to SPI-
282 based drought, with regions such as northern Africa, the Mediterranean, the Middle East and
283 central China being the most affected, while only very small regions in high northern latitudes
284 show decreases in drought occurrence based on this measure (Figure 2c). This much wider
285 spread of drought increases is also reflected in the global average time series, which show
286 upward trends from about 2015 to 2100 under all scenarios, with SSP5-8.5 being the one with
287 the largest increases and SSP1-2.6 becoming stationary from about the 2050s. The other two
288 scenarios, SSP3-7.0 and SSP2-4.5, lie between the two (Figure 2d, Table S3), again indicating a
289 proportionality of the global drought response to the strength of forcing. Such a larger increase in
290 dryness from *spei3_dry* compared to *spi3_dry* is expected as with warming temperatures also the
291 atmospheric water demand increases (e.g. Pall et al., 2007).

292
293 The difference maps for the other *spi3_dry* and *spei3_dry* SSP scenarios have similar spatial
294 patterns as shown in Figure 2a,c. However, from SSP3-7.0 to SSP1-2.6, we note that for
295 *spi3_dry* the areas with decreasing drought occurrences increase (Figure S12), whereas for
296 *spei3_dry* the areas with increasing drought counts decrease in scenarios with weaker forcing
297 (Figure S13).

298
299 The difference maps for *spi6_dry*, *spei6_dry*, *spi12_dry* and *spei12_dry* show very similar
300 patterns as found in Figure 2a,c, however the statistical significance is sometimes lower,
301 especially for the *spi12_dry* and *spei12_dry* (Figures S14-S17). The global average time-series
302 computed for the same dry extremes indices are also very similar to those found for *spi3_dry* and
303 *spei3_dry* (Figure S18, Table S3).

304
305 **3.3 Compound hot-dry extremes**

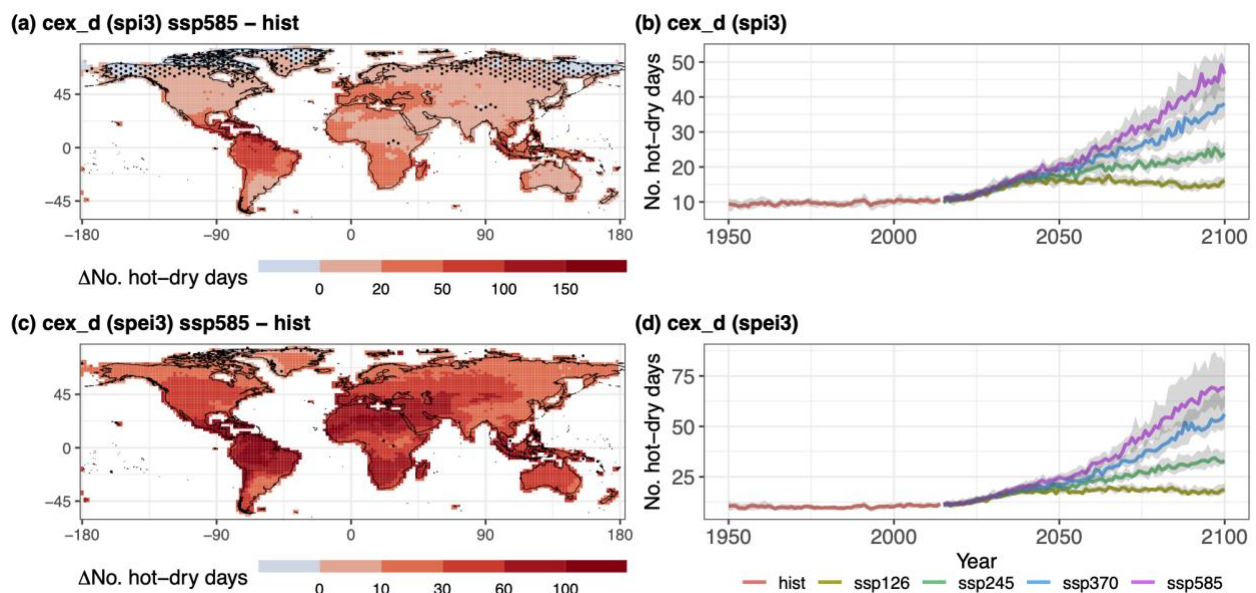
306 The end-of-century changes for compound hot-dry extremes, under the SSP5-8.5 show a
307 widespread increase in the occurrence of such events (Figure 3a,c). For *cex_d (spi3)* the regions
308 showing stronger increase in compound hot-dry extremes are central and northern South
309 America, central Europe, the Mediterranean, western and southern Africa and Indonesia (Figure
310 3a). Compound hot-dry extremes computed with *cex_d (spei3)* show large increases over the
311 same areas mentioned above but also in northern Africa and the Middle East (Figure 3c). For
312 *cex_d (spi3)* there are areas in high northern latitudes with no increase in compound extremes
313 and this is related to the decreased drought frequency in these regions (Figures 3a and 2a). On
314 the other hand, *cex_d (spei3)* shows significant increases globally (Figure 3b). When looking at
315 the climatologies (1981-2010) of compound hot-dry extremes for both *cex_d (spi3)* and *cex_d*
316 (*spei3*) we notice that the regions where compound extremes occur more frequently under
317 current conditions do not necessarily match with the regions where we obtain larger changes by
318 the end of the 21st century (Figures 2a,c; S19-S20).

319
320 In accordance with the difference maps of both *cex_d (spi3)* and *cex_d (spei3)*, also the median
321 of annual and global average time-series show strong monotonic and positive trends for all the
322 SSP scenarios from about 2015 to 2100, except for the SSP1-2.6 in which the compound extreme
323 occurrences stabilize around the 2050s ($p < 0.01$, Table S4). As for the univariate extremes
324 presented in the previous sections, the SSP5-8.5 is the scenario with the strongest increases,

325 followed by SSP3-7.0, SSP2-4.5 and SSP1-2.6 (Figure 3b,d) and changes in compound extremes
 326 computed with SPEI to detect drought are much stronger than extremes computed with SPI.

327
 328 The $cex_d(spi3)$ and $cex_d(spei3)$ difference maps computed for the other SSP scenarios show
 329 similar changes as for SSP5-8.5, although the magnitudes and statistical significance are reduced
 330 from SSP3-7.0 to SSP1-2.6 (Figures S21-S22). Also the difference maps of $cex_d(spi6)$ ($spei6$)
 331 ($spi12$) and ($spei12$) reflect the changes similar to $cex_d(spi3)$ and ($spei3$), with both magnitude
 332 and statistical significance reduced from SSP5-8.5 to SSP1-2.6 and from $cex_d(spi12, spei12)$ to
 333 $cex_d(spi3, spei3)$ (Figures S23-S26). Lastly, the annual global average time-series for the other
 334 cex_d indices computed with $spi6$, $spei6$, $spi12$ and $spei12$ also show similar characteristics as
 335 $cex_d(spi3)$ and $cex_d(spei3)$ (Figure S27, Table S4).

336
 337



338
 339 **Figure 3.** MME difference maps and global land average time-series of compound hot-dry extremes. (a)-
 340 (b) Annual number of compound hot-dry extremes computed with daily maximum near-surface
 341 temperature and SPI3. (c)-(d) same as (a)-(b) but with SPEI3. Time-periods, stippling and time-series
 342 colors are as in Figure 1.

343
 344

345 4 Discussion and conclusions

346 Our results show significant projected increases in the frequency, intensity and duration of hot
 347 extremes in most regions by the end of the 21st century, and these increases are strongest for the
 348 SSP5-8.5 scenario and weakest for SSP1-2.6. Such increase in hot extremes reflect the findings
 349 of other studies (e.g. Christidis et al., 2015; Fischer & Schär, 2010; Mukherjee et al., 2022; Yin
 350 et al., 2022) but can differ from other studies using different temperature extreme indices (e.g.
 351 Saeed et al., 2021).

352
 353 Dry extremes, on the other hand, show different regional patterns of change depending on the
 354 index used to measure drought (i.e. SPI or SPEI). Such a difference is related to the types of
 355 variables included in the indices (e.g. precipitation or precipitation and PET) (Dai, 2011, 2013).
 356 While there is sensitivity to the specific measures to detect drought, the results are fairly robust

357 for different drought accumulation periods (i.e. 3, 6 and 12 months). Dry extremes computed
358 with SPI, under SSP5-8.5, increase over central and northern South America, the Mediterranean,
359 southern Africa and western Australia and decrease over China and in the high northern
360 latitudes. On the other hand, dry extremes computed with SPEI show consistent increase
361 generally all over the globe, but especially in the Mediterranean, northern Africa, the Middle
362 East and central China. Our results reflect the expectation that evaporative demand of the
363 atmosphere increases at higher temperatures, and this is a driver of drought when characterized
364 with SPEI. When assessing the global land average time-series, regional drought increases and
365 decreases computed with SPI partly compensate each other and global average increases in
366 drought only occur in the strongest forcing scenarios. On the other hand, the global land averages
367 affected by drought computed with SPEI increase in all scenarios. The increase in dryness can be
368 primarily driven by the changing patterns of precipitation (when based on SPI) and additionally
369 by the increasing atmospheric water demand as the climate warms (when based on SPEI).

370

371 Results for compound hot-dry extremes are consistent with the changes in univariate hot and dry
372 extremes and therefore the difference maps for SSP5-8.5 point toward widespread increases in
373 compound hot-dry extremes for indices computed with both SPI ($cex_d(spi3)$, $cex_d(spi6)$ and
374 $cex_d(spi12)$) and SPEI ($cex_d(spei3)$, $cex_d(spei6)$ and $cex_d(spei12)$). These widespread
375 increases are therefore also reflected in the global land average time series, indicating significant
376 increases by the end of the 21st century in all four scenarios.

377

378 Our findings allow a direct comparison between univariate and compound hot-dry extremes and
379 are in accordance with other studies pointing towards an increase in hot-dry compound extremes
380 under anthropogenic climate change. For instance, Bevacqua et al. (2022) found a projected
381 increase in hot-dry extremes and assessed their uncertainty but only using precipitation as a
382 proxy for dry events. Similarly, Hao et al. (2018) and Ridder et al. (2022) computed dry
383 extremes only from precipitation and the latter study used Excess Heat Factor for assessing
384 heatwaves. Our results show that there is some sensitivity in the projected changes with respect
385 to dry and compound hot-dry extremes, attributed to the way dry extremes are measured.

386

387 Our analysis framework provides insights from considering the different univariate and
388 compound indices in combination. In particular we find that global increases in hot extremes
389 alone are driving the increase in compound extremes in regions where dry extremes, computed
390 with SPI, decrease (e.g. northern Europe and China). On the contrary, compound extremes
391 computed with SPEI (and computed with SPI in regions where drought becomes more frequent)
392 are increasing because of the contributions of increasing both univariate hot and dry extremes.
393 The pattern in compound extremes computed with SPI is also in agreement with Bevacqua et al.
394 (2022), who highlighted the role of regional precipitation in driving future changes in compound
395 hot-dry extremes. As limitations, we did not take into account models' uncertainty driven by
396 internal climate variability (Deser, 2020) and dry extremes were computed from the SPI and
397 SPEI indices at ≥ 3 months accumulation periods so that we may have lost the representation of
398 short dry spells and with a 12-month accumulation, seasonality was implicitly removed.

399

400 In summary, we provide a comprehensive global analysis of compound hot-dry extreme changes
401 in the context of the corresponding univariate hot and dry extremes for 25 CMIP6 models and
402 four SSP scenarios. We specifically show that the entire set of extremes are projected to increase

403 in the future under the highest emission scenario (SSP5-8.5) and that such increase could be
 404 partly mitigated under the lowest emission scenario (SSP1-2.6). We conclude that the risk of hot
 405 and dry extremes will significantly increase in the next decades in many regions, and encourage
 406 particular attention from governments and stakeholders worldwide to implement suitable
 407 adaptation measures and put into practice strong mitigation policies to limit the increases of such
 408 events.

409
 410

411 **Acknowledgements**

412 This study is a contribution to the Horizon2020 LANDMARC project, and has been carried out
 413 with funding from this grant (grant agreement No. 869367). PDL has also received funding from
 414 the European Union's Horizon Europe Research and Innovation Programme under grant
 415 agreement No 101059659. The authors would like to thank Margarida Samso-Cabre for
 416 downloading, storing and reformatting the CMIP6 data used in the analyses.

417
 418

419 **Open Research**

420 The CMIP6 data are freely available and have been downloaded from the Earth System Grid
 421 Federation (ESGF) website (<https://esgf-node.llnl.gov/search/cmip6/>). We compute the ClimImpact
 422 (<https://climimpact-sci.org/>) univariate extreme indices using the R packages “*climindex.pcic.ncdf*”
 423 (<https://github.com/ARCCSS-extremes/climindex.pcic.ncdf>) and “SPEI”
 424 (<https://github.com/sbegueria/SPEI>; Beguería et al., 2014).

425
 426

427 **References**

- 428 Allen, R. G., Smith, M., Pereira, L. S., & Perrier, A. (1994). An update for the calculation of reference
 429 evapotranspiration. *ICID Bul.*, *43*(2), 35–92.
- 430 Barriopedro, D., Fischer, E. M., Luterbacher, J., Trigo, R. M., & García-Herrera, R. (2011). The Hot Summer of
 431 2010: Redrawing the Temperature Record Map of Europe. *Science (New York, N.Y.)*, *332*(6026), 220–224.
- 432 Beguería, S., Vicente-Serrano, S. M., Reig, F., & Latorre, B. (2014). Standardized precipitation evapotranspiration
 433 index (SPEI) revisited: parameter fitting, evapotranspiration models, tools, datasets and drought monitoring.
 434 *International Journal of Climatology*, *34*(10), 3001–3023. <https://doi.org/https://doi.org/10.1002/joc.3887>
- 435 Bevacqua, E., Zappa, G., Lehner, F., & Zscheischler, J. (2022). Precipitation trends determine future occurrences of
 436 compound hot–dry events. *Nature Climate Change*, *12*(4), 350–355. [https://doi.org/10.1038/s41558-022-](https://doi.org/10.1038/s41558-022-01309-5)
 437 [01309-5](https://doi.org/10.1038/s41558-022-01309-5)
- 438 Bonferroni, C. (1936). Teoria statistica delle classi e calcolo delle probabilità. *Pubblicazioni Del R. Istituto*
 439 *Superiore Di Scienze Economiche e Commerciali Di Firenze*, *8*, 3–62.
- 440 Christidis, N., Jones, G. S., & Stott, P. A. (2015). Dramatically increasing chance of extremely hot summers since
 441 the 2003 European heatwave. *Nature Climate Change*, *5*(1), 46–50. <https://doi.org/10.1038/nclimate2468>
- 442 Cook, B. I., Mankin, J. S., & Anchukaitis, K. J. (2018). Climate Change and Drought: From Past to Future. *Current*
 443 *Climate Change Reports*, *4*(2), 164–179. <https://doi.org/10.1007/s40641-018-0093-2>
- 444 Dai, A. (2011). Drought under global warming: A review. *Wiley Interdisciplinary Reviews: Climate Change*, *2*(1),
 445 45–65. <https://doi.org/10.1002/wcc.81>
- 446 Dai, A. (2013). Increasing drought under global warming in observations and models. *Nature Climate Change*, *3*(1),
 447 52–58. <https://doi.org/10.1038/nclimate1633>
- 448 Deser, C. (2020). “Certain Uncertainty: The Role of Internal Climate Variability in Projections of Regional Climate
 449 Change and Risk Management.” *Earth’s Future*, *8*(12), e2020EF001854.
 450 <https://doi.org/https://doi.org/10.1029/2020EF001854>
- 451 Donat, M. G., Pitman, A. J., & Seneviratne, S. I. (2017). Regional warming of hot extremes accelerated by surface
 452 energy fluxes. *Geophysical Research Letters*, *44*(13), 7011–7019.
 453 <https://doi.org/https://doi.org/10.1002/2017GL073733>

- 454 Eyring, V., Bony, S., Meehl, G. A., Senior, C. A., Stevens, B., Stouffer, R. J., & Taylor, K. E. (2016). Overview of
455 the Coupled Model Intercomparison Project Phase 6 (CMIP6) experimental design and organization. *Geosci.*
456 *Model Dev.*, 9(5), 1937–1958. <https://doi.org/10.5194/gmd-9-1937-2016>
- 457 Fischer, E. M., & Schär, C. (2010). Consistent geographical patterns of changes in high-impact European heatwaves.
458 *Nature Geoscience*, 3, 398.
- 459 Ganguli, P. (2023). Amplified risk of compound heat stress-dry spells in Urban India. *Climate Dynamics*, 60(3),
460 1061–1078. <https://doi.org/10.1007/s00382-022-06324-y>
- 461 Hamed, K. H., & Ramachandra Rao, A. (1998). A modified Mann-Kendall trend test for autocorrelated data.
462 *Journal of Hydrology*, 204(1), 182–196. [https://doi.org/https://doi.org/10.1016/S0022-1694\(97\)00125-X](https://doi.org/10.1016/S0022-1694(97)00125-X)
- 463 Hao, Z., Hao, F., Singh, V. P., & Zhang, X. (2018). Changes in the severity of compound drought and hot extremes
464 over global land areas. *Environmental Research Letters*, 13(12), 124022. [https://doi.org/10.1088/1748-](https://doi.org/10.1088/1748-9326/aace96)
465 [9326/aace96](https://doi.org/10.1088/1748-9326/aace96)
- 466 Hargreaves, G. H. (1994). Defining and Using Reference Evapotranspiration. *Journal of Irrigation and Drainage*
467 *Engineering*, 120(6), 1132–1139. [https://doi.org/10.1061/\(ASCE\)0733-9437\(1994\)120:6\(1132\)](https://doi.org/10.1061/(ASCE)0733-9437(1994)120:6(1132))
- 468 Horton, D. E., Johnson, N. C., Singh, D., Swain, D. L., Rajaratnam, B., & Diffenbaugh, N. S. (2015). Contribution
469 of changes in atmospheric circulation patterns to extreme temperature trends. *Nature*, 522(7557), 465–9.
- 470 De Luca, P., Messori, G., Wilby, R. L., Mazzoleni, M., & Di Baldassarre, G. (2020). Concurrent wet and dry
471 hydrological extremes at the global scale. *Earth Syst. Dynam.*, 11(1), 251–266. [https://doi.org/10.5194/esd-](https://doi.org/10.5194/esd-11-251-2020)
472 [11-251-2020](https://doi.org/10.5194/esd-11-251-2020)
- 473 De Luca, P., Messori, G., Pons, F. M. E., & Faranda, D. (2020). Dynamical Systems Theory Sheds New Light on
474 Compound Climate Extremes in Europe and Eastern North America. *Quarterly Journal of the Royal*
475 *Meteorological Society*, (146), 1636–1650. <https://doi.org/10.1002/qj.3757>
- 476 Mann, H. B., & Whitney, D. R. (1947). On a Test of Whether one of Two Random Variables is Stochastically
477 Larger than the Other. *Ann. Math. Statist.*, 18(1), 50–60. <https://doi.org/10.1214/aoms/1177730491>
- 478 Manning, C., Widmann, M., Bevacqua, E., Van Loon, A. F., Maraun, D., & Vrac, M. (2019). Increased probability
479 of compound long-duration dry and hot events in Europe during summer (1950–2013). *Environmental*
480 *Research Letters*, 14(9), 94006. <https://doi.org/10.1088/1748-9326/ab23bf>
- 481 Masson-Delmotte, V., Zhai, P., Pirani, A., Connors, S. L., Péan, C., Berger, S., et al. (2021). *IPCC, 2021: Summary*
482 *for Policymakers. In: Climate Change 2021: The Physical Science Basis. Contribution of Working Group I to*
483 *the Sixth Assessment Report of the Intergovernmental Panel on Climate Change*. Cambridge University Press,
484 Cambridge, United Kingdom and New York, NY, USA.
- 485 McKee, T. B., Doesken, N. J., & Kleist, J. (1993). The relationship of drought frequency and duration to time scales.
486 In *AMS 8th Conference on Applied Climatology* (pp. 179–184). Anaheim: AMS 8th Conference on Applied
487 Climatology.
- 488 Mukherjee, S., Mishra, A. K., Ashfaq, M., & Kao, S.-C. (2022). Relative effect of anthropogenic warming and
489 natural climate variability to changes in Compound drought and heatwaves. *Journal of Hydrology*, 605,
490 127396. [https://doi.org/https://doi.org/10.1016/j.jhydrol.2021.127396](https://doi.org/10.1016/j.jhydrol.2021.127396)
- 491 Mukherjee, S., Mishra, A. K., Zscheischler, J., & Entekhabi, D. (2023). Interaction between dry and hot extremes at
492 a global scale using a cascade modeling framework. *Nature Communications*, 14(1), 277.
493 <https://doi.org/10.1038/s41467-022-35748-7>
- 494 O'Neill, B. C., Tebaldi, C., van Vuuren, D. P., Eyring, V., Friedlingstein, P., Hurtt, G., et al. (2016). The Scenario
495 Model Intercomparison Project (ScenarioMIP) for CMIP6. *Geosci. Model Dev.*, 9(9), 3461–3482.
496 <https://doi.org/10.5194/gmd-9-3461-2016>
- 497 Pall, P., Allen, M. R., & Stone, D. A. (2007). Testing the Clausius–Clapeyron constraint on changes in extreme
498 precipitation under CO2 warming. *Climate Dynamics*, 28(4), 351–363. [https://doi.org/10.1007/s00382-006-](https://doi.org/10.1007/s00382-006-0180-2)
499 [0180-2](https://doi.org/10.1007/s00382-006-0180-2)
- 500 Palmer, W. (1965). Meteorological Drought. *US Weather Bur., US Res. Pa.*(Washington, D.C.).
- 501 Perkins-Kirkpatrick, S. E., & Lewis, S. C. (2020). Increasing trends in regional heatwaves. *Nature Communications*,
502 11(1), 3357. <https://doi.org/10.1038/s41467-020-16970-7>
- 503 Perkins, S. E., & Alexander, L. V. (2013). On the Measurement of Heat Waves. *Journal of Climate*, 26(13), 4500–
504 4517. <https://doi.org/10.1175/JCLI-D-12-00383.1>
- 505 Rastogi, D., Lehner, F., & Ashfaq, M. (2020). Revisiting Recent U.S. Heat Waves in a Warmer and More Humid
506 Climate. *Geophysical Research Letters*, 47(9), e2019GL086736.
507 [https://doi.org/https://doi.org/10.1029/2019GL086736](https://doi.org/10.1029/2019GL086736)
- 508 Ridder, N. N., Ukkola, A. M., Pitman, A. J., & Perkins-Kirkpatrick, S. E. (2022). Increased occurrence of high
509 impact compound events under climate change. *Npj Climate and Atmospheric Science*, 5(1), 3.

- 510 <https://doi.org/10.1038/s41612-021-00224-4>
- 511 Rousi, E., Kornhuber, K., Beobide-Arsuaga, G., Luo, F., & Coumou, D. (2022). Accelerated western European
512 heatwave trends linked to more-persistent double jets over Eurasia. *Nature Communications*, *13*(1), 3851.
513 <https://doi.org/10.1038/s41467-022-31432-y>
- 514 Saeed, F., Schleussner, C.-F., & Ashfaq, M. (2021). Deadly Heat Stress to Become Commonplace Across South
515 Asia Already at 1.5°C of Global Warming. *Geophysical Research Letters*, *48*(7), e2020GL091191.
516 <https://doi.org/https://doi.org/10.1029/2020GL091191>
- 517 Schielicke, L., & Pfahl, S. (2022). European heatwaves in present and future climate simulations: A Lagrangian
518 analysis. *Weather Clim. Dynam. Discuss.*, *2022*, 1–36. <https://doi.org/10.5194/wcd-2022-45>
- 519 Schubert, S. D., Stewart, R. E., Wang, H., Barlow, M., Berbery, E. H., Cai, W., et al. (2016). Global Meteorological
520 Drought: A Synthesis of Current Understanding with a Focus on SST Drivers of Precipitation Deficits.
521 *Journal of Climate*, *29*(11), 3989–4019. <https://doi.org/10.1175/JCLI-D-15-0452.1>
- 522 Sedgwick, P. (2014). Multiple hypothesis testing and Bonferroni's correction. *BMJ: British Medical Journal*, *349*,
523 g6284. <https://doi.org/10.1136/bmj.g6284>
- 524 Sen, P. K. (1968). Estimates of the Regression Coefficient Based on Kendall's Tau. *Journal of the American*
525 *Statistical Association*, *63*(324), 1379–1389. <https://doi.org/10.1080/01621459.1968.10480934>
- 526 Seneviratne, S. I., Lüthi, D., Litschi, M., & Schär, C. (2006). Land–atmosphere coupling and climate change in
527 Europe. *Nature*, *443*(7108), 205–209. <https://doi.org/10.1038/nature05095>
- 528 Seneviratne, S. I., Donat, M. G., Pitman, A. J., Knutti, R., & Wilby, R. L. (2016). Allowable CO2 emissions based
529 on regional and impact-related climate targets. *Nature*, *529*(7587), 477–483.
530 <https://doi.org/10.1038/nature16542>
- 531 Sippel, S., Zscheischler, J., Heimann, M., Otto, F. E. L., Peters, J., & Mahecha, M. D. (2015). Quantifying changes
532 in climate variability and extremes: Pitfalls and their overcoming. *Geophysical Research Letters*, *42*(22),
533 9990–9998. <https://doi.org/https://doi.org/10.1002/2015GL066307>
- 534 Suarez-Gutierrez, L., Müller, W. A., Li, C., & Marotzke, J. (2020). Dynamical and thermodynamical drivers of
535 variability in European summer heat extremes. *Climate Dynamics*, *54*(9), 4351–4366.
536 <https://doi.org/10.1007/s00382-020-05233-2>
- 537 Teuling, A. J., Van Loon, A. F., Seneviratne, S. I., Lehner, I., Aubinet, M., Heinesch, B., et al. (2013).
538 Evapotranspiration amplifies European summer drought. *Geophysical Research Letters*, *40*(10), 2071–2075.
539 <https://doi.org/https://doi.org/10.1002/grl.50495>
- 540 Thornthwaite, C. W. (1948). An Approach toward a Rational Classification of Climate. *Geographical Review*, *38*(1),
541 55–94. <https://doi.org/10.2307/210739>
- 542 Trenberth, K. E., Dai, A., van der Schrier, G., Jones, P. D., Barichivich, J., Briffa, K. R., & Sheffield, J. (2014).
543 Global warming and changes in drought. *Nature Climate Change*, *4*(1), 17–22.
544 <https://doi.org/10.1038/nclimate2067>
- 545 Ukkola, A. M., De Kauwe, M. G., Roderick, M. L., Abramowitz, G., & Pitman, A. J. (2020). Robust Future
546 Changes in Meteorological Drought in CMIP6 Projections Despite Uncertainty in Precipitation. *Geophysical*
547 *Research Letters*, *47*(11), e2020GL087820. <https://doi.org/https://doi.org/10.1029/2020GL087820>
- 548 Vicente-Serrano, S. M., Beguería, S., & López-Moreno, J. I. (2010). A Multiscalar Drought Index Sensitive to
549 Global Warming: The Standardized Precipitation Evapotranspiration Index. *Journal of Climate*, *23*(7), 1696–
550 1718. <https://doi.org/10.1175/2009JCLI2909.1>
- 551 Vicente-Serrano, S. M., Domínguez-Castro, F., McVicar, T. R., Tomas-Burguera, M., Peña-Gallardo, M., Noguera,
552 I., et al. (2020). Global characterization of hydrological and meteorological droughts under future climate
553 change: The importance of timescales, vegetation-CO2 feedbacks and changes to distribution functions.
554 *International Journal of Climatology*, *40*(5), 2557–2567. <https://doi.org/https://doi.org/10.1002/joc.6350>
- 555 Vogel, M. M., Zscheischler, J., Fischer, E. M., & Seneviratne, S. I. (2020). Development of Future Heatwaves for
556 Different Hazard Thresholds. *Journal of Geophysical Research: Atmospheres*, *125*(9), e2019JD032070.
557 <https://doi.org/https://doi.org/10.1029/2019JD032070>
- 558 Vogel, M. M., Hauser, M., & Seneviratne, S. I. (2020). Projected changes in hot, dry and wet extreme events'
559 clusters in CMIP6 multi-model ensemble. *Environmental Research Letters*, *15*(9), 94021.
560 <https://doi.org/10.1088/1748-9326/ab90a7>
- 561 Wu, H., Svoboda, M. D., Hayes, M. J., Wilhite, D. A., & Wen, F. (2007). Appropriate application of the
562 standardized precipitation index in arid locations and dry seasons. *International Journal of Climatology*, *27*(1),
563 65–79. <https://doi.org/https://doi.org/10.1002/joc.1371>
- 564 Wu, X., Hao, Z., Hao, F., Singh, V. P., & Zhang, X. (2019). Dry-hot magnitude index: a joint indicator for
565 compound event analysis. *Environmental Research Letters*, *14*(6), 64017. <https://doi.org/10.1088/1748->

- 566 9326/ab1ec7
567 Yin, J., Slater, L., Gu, L., Liao, Z., Guo, S., & Gentine, P. (2022). Global Increases in Lethal Compound Heat
568 Stress: Hydrological Drought Hazards Under Climate Change. *Geophysical Research Letters*, 49(18),
569 e2022GL100880. <https://doi.org/https://doi.org/10.1029/2022GL100880>
- 570 Yu, B., Li, G., Chen, S., & Lin, H. (2020). The role of internal variability in climate change projections of North
571 American surface air temperature and temperature extremes in CanESM2 large ensemble simulations. *Climate*
572 *Dynamics*, 55(3), 869–885. <https://doi.org/10.1007/s00382-020-05296-1>
- 573 Zhang, X., Alexander, L., Hegerl, G. C., Jones, P., Tank, A. K., Peterson, T. C., et al. (2011). Indices for monitoring
574 changes in extremes based on daily temperature and precipitation data. *WIREs Climate Change*, 2(6), 851–
575 870. <https://doi.org/https://doi.org/10.1002/wcc.147>
- 576 Zhang, Y., Hao, Z., Feng, S., Zhang, X., & Hao, F. (2022). Changes and driving factors of compound agricultural
577 droughts and hot events in eastern China. *Agricultural Water Management*, 263, 107485.
578 <https://doi.org/https://doi.org/10.1016/j.agwat.2022.107485>
- 579 Zscheischler, J., & Fischer, E. M. (2020). The record-breaking compound hot and dry 2018 growing season in
580 Germany. *Weather and Climate Extremes*, 29, 100270.
581 <https://doi.org/https://doi.org/10.1016/j.wace.2020.100270>
- 582 Zscheischler, J., Westra, S., van den Hurk, B. J. J. M., Seneviratne, S. I., Ward, P. J., Pitman, A., et al. (2018).
583 Future climate risk from compound events. *Nature Climate Change*, 8(6), 469–477.
584 <https://doi.org/10.1038/s41558-018-0156-3>
- 585 Zscheischler, J., Martius, O., Westra, S., Bevacqua, E., Raymond, C., Horton, R. M., et al. (2020). A typology of
586 compound weather and climate events. *Nature Reviews Earth & Environment*. [https://doi.org/10.1038/s43017-](https://doi.org/10.1038/s43017-020-0060-z)
587 020-0060-z
588